



Article

Algorithm to Predict the Rainfall Starting Point as a Function of Atmospheric Pressure, Humidity, and Dewpoint

Alfonso Gutierrez-Lopez ^{1,*} , Ivonne Cruz-Paz ² and Martin Muñoz Mandujano ² 

¹ Water Research Center, Centro de Investigaciones del Agua-Queretaro (CIAQ), International Flood Initiative, Latin-American and the Caribbean Region (IFI-LAC), International Hydrological Programme (IHP-UNESCO), Universidad Autonoma de Queretaro, Queretaro 76010, Mexico

² Facultad de Informatica, Universidad Autonoma de Queretaro, Juriquilla Queretaro 76230, Mexico; icruz23@alumnos.uaq.mx (I.C.-P.); mmunoz23@alumnos.uaq.mx (M.M.M.)

* Correspondence: alfonso.gutierrez@uaq.mx; Tel.: +52-442-192-1200 (ext. 6401)

Received: 24 September 2019; Accepted: 23 October 2019; Published: 12 November 2019



Abstract: Forecasting extreme precipitations is one of the main priorities of hydrology in Latin America and the Caribbean (LAC). Flood damage in urban areas increases every year, and is mainly caused by convective precipitations and hurricanes. In addition, hydrometeorological monitoring is limited in most countries in this region. Therefore, one of the primary challenges in the LAC region the development of a good rainfall forecasting model that can be used in an early warning system (EWS) or a flood early warning system (FEWS). The aim of this study was to provide an effective forecast of short-term rainfall using a set of climatic variables, based on the Clausius–Clapeyron relationship and taking into account that atmospheric water vapor is one of the variables that determine most meteorological phenomena, particularly regarding precipitation. As a consequence, a simple precipitation forecast model was proposed from data monitored at every minute, such as humidity, surface temperature, atmospheric pressure, and dewpoint. With access to a historical database of 1237 storms, the proposed model allows use of the right combination of these variables to make an accurate forecast of the time of storm onset. The results indicate that the proposed methodology was capable of predicting precipitation onset as a function of the atmospheric pressure, humidity, and dewpoint. The synoptic forecast model was implemented as a hydroinformatics tool in the Extreme Precipitation Monitoring Network of the city of Queretaro, Mexico (RedCIAQ). The improved forecasts provided by the proposed methodology are expected to be useful to support disaster warning systems all over Mexico, mainly during hurricanes and flashfloods.

Keywords: humidity; dewpoint; rainfall; mixing ratio; forecast rainfall model; Clausius–Clapeyron relation; early warning system (EWS); Mexico

1. Introduction

In Mexico, as in most Latin American and Caribbean (LAC) countries, there is a deficit of historical precipitation data measured in time intervals of less than 24 h. Real-time measured values are often required for the implementation of early warning systems. In Mexico, disasters are measured by the economic impact of damage and losses, as well as by the problems caused in the social environment, such as injured and dead people and damaged houses, schools, and hospitals, among other issues. From 2000 to 2014, 2147 million dollars' worth of losses and 186 annual deaths occurred [1]. The year 2013 was very intense in terms of rainfall, especially the month of September, and the historical precipitation depth increased by 60% with respect to the historical mean, registering a monthly mean

of 227.3 mm and exceeding the 1955 record of 212.1 mm [2]. Weather predictions consist of several variables, such as temperature, humidity, wind, dewpoint, among others, trying to provide a suitable and accurate forecast. However, forecasting difficulties arise often because of the small scales involved, the range of responsible physical mechanisms, and the challenge involved in forecasting events of such short duration. The first piece of evidence is the relationship between the natural logarithm of the rainfall with the surface temperature, indicating an exponential behavior [3]. Additionally, it is necessary to point out that precipitation is episodic and does not have continuous values like temperature and other climate variables; therefore, it is noticeable that anticipating the occurrence of precipitation is difficult. Lorenz and Saltzman [4–6] were perhaps the first to perceive that climate is a complex, nonlinear system involving both deterministic and stochastic components. However, the basic idea that the origin of convective precipitation as a function of surface temperature was demonstrated by [7], who used temperature and rain gauge station data of 5-min accumulation intervals. This strong relationship with temperature also implies the relationship with convective available potential energy (CAPE) magnitude. Therefore, it is accepted that the main variables for predicting precipitation are temperature and humidity [8]. Nevertheless, there are other four meteorological parameters—air, dewpoint temperature (or relative humidity), wind speed, and cloud cover—which are strongly correlated with rainfall [9]. Scientific studies are known to show that there is an increase in precipitation intensity due to temperature gradient. In particular, subdaily or hourly precipitation exhibits an improved correlation with thermodynamic constraints, known as the Clausius–Clapeyron (C–C) relation [10]. It has also been confirmed that this phenomenon occurs with different types of precipitation, i.e., with orographic precipitation and convective precipitation [11]. Concerning tropical regions, [12] showed that 30 years ago, the surface temperature was an important meteorological variable to the understanding of tropical weather systems. This was one of the first studies to use temperature gradients to carry out dust haze forecasting. Since 1990, the multivariate statistical studies of 28 different climatic variables in Australia have shown that the main factors for creating a climatic model are a humidity factor, a temperature factor, and a rainfall factor [13].

An acceptable forecast of precipitation intensity is an essential issue in the forecasts of extreme streamflow events [14]. The research to date has tended to focus on hydrometeorological data, such as wind, temperature, humidity, and atmospheric pressure; this information has been used in a daily streamflow forecast during lead times of 5–7 days [15]. However, the purpose of an early warning system (EWS), flood early warning system (FEWS), or an ensemble prediction system (EPS) is to allow warning signals prior to extreme events mainly for very short-term heavy rainfall. Recent developments in machine learning techniques have heightened the need of using the mentioned hydrometeorological data for an effective EWS for very short-term (heavy rain advisory within the next 3–9 h) [16]. Nevertheless, we must accept that short-term quantitative precipitation forecasting (SQPF) is critical for flashflood warning, navigation safety, and many other applications. Zahraei et al. [17] have recently developed a methodology based on the method named PERsiann-ForeCAST. PERCAST predicts the location and rate of rainfall up to 4 h using the most recent storm images to extract the storm features.

Recent evidence suggests that a forecasting model that includes a radar-based nowcasting component is capable of predicting rainfall distribution patterns of 1–2 h for rainstorms of moderate to heavy intensity (30–50 mm/h) [18]. However, difficulties arise when an attempt is made to implement the SQPF, especially when talking about models that can be used to simulate hydrological processes at a daily or hourly time step, because one major drawback of this approach is the large spatial variation in precipitation [19]. The changes experienced by hydroinformatics tools over the past decade remain unprecedented. Many analysts now argue that the strategy of introducing more hourly surface data, including on wind, specific humidity (dewpoint), air temperature, relative vorticity, and moisture divergence flux, has been successful when it is combined with a Bayesian framework [20] or a neural network used to generate rainfall forecast for the next time step [21]. Not only is it important to know the variables that generate rain but, also, it is important to find the right combination of these variables

to make an accurate forecast of the starting time of a storm. From the abovementioned, it is concluded that one of the most important tasks of modern hydrology is to work on simple and effective models in the forecasting of extreme events. The objective of this work is to present a simple forecast model for precipitation onset, called CRHUDA (CRossingHUmidity, Dewpoint, and Atmospheric pressure) based on measurements of humidity, atmospheric pressure, and dewpoint that are taken every minute.

2. Materials and Methods

2.1. The Clausius–Clapeyron Relation

In nature, water has three states, but each state depends mainly on temperature and pressure [22]. The transformation of water from solid to liquid is known as the fusion point, and the process of transition from solid to gas is called sublimation [23]. The absolute pressure at which water passes from liquid to gas is known as vapor pressure, and this transformation occurs at a temperature called the boiling point [24].

The term humidity is used a lot when talking about present moisture in the atmosphere. The partial pressure exerted by water molecules may increase until a certain limit is reached, at this threshold, the number of water molecules evaporating from the liquid equals the number of those returning from the atmosphere, establishing a dynamic balance between evaporation and condensation, called saturation. The saturation threshold is determined by the temperature T , but it is independent of the dry air pressure [25]. If, in this complete process, there is a change in the pressure ΔP [26], it is because there is some work, W , which will be equal to the latent heat C multiplied by the change in temperature ΔT [27]. This can be shown as

$$\Delta W = C \frac{\Delta T}{T} \quad (1)$$

On the other hand, in order for any change of state to take place, it is necessary to change the specific volume, i.e., a differential of the volumes from gas (V_g) to liquid (V_l) [28,29].

$$W = \Delta P (V_g - V_l) \quad (2)$$

By equating Equations (1) and (2),

$$\frac{\Delta P}{\Delta T} = \frac{\partial P}{\partial T} = \frac{C}{T \Delta V}. \quad (3)$$

This formulation for the latent heat of vaporization was deduced by Clapeyron from Carnot's theory, and was proved by Clausius. This relation is used to calculate C at any temperature when the specific volumes and the relationship between the increase of saturation pressure and T , are known [25]. This equation is known as the Clausius–Clapeyron relationship (C–C), and it characterizes the behavior of a closed system during a phase change [30,31], where temperature and pressure are constants by definition [32].

The basic hypothesis of the C–C relation is that as the temperature increases, relative humidity remains constant and specific humidity increases after the increase of moisture availability in the atmosphere [10]. In some tropical regions, the total precipitation increase may be greater than that predicted by the Clausius–Clapeyron relation and, thus, a different compensating response is required [33]. Certainly, the prediction of precipitation must be based on the adequate and detailed use of the relationship C–C. This view is supported by [34], who write “*present-day precipitation-temperature scaling relations indicate that hourly precipitation extremes may have a response to warming exceeding the Clausius–Clapeyron relation*”. This is simple to see on a graph, since it is usually presented as temperature ($1/T$) vs. pressure ($\ln P$) [35,36]. In [37], 11 different rules can be proposed for deduction of Equation (3). To date, various methods (studies) have been developed and introduced to find the C–C relation between subdaily extreme precipitation and daily mean temperature [10].

The dewpoint temperature, T_d , is the temperature at which the air is saturated if it is cooled at constant pressure [38]. T_d is the temperature at which the vapor pressure is equal to the saturation pressure of the air (water vapor mixing ratio). In the same way, the vapor volume presented in the atmosphere can be expressed through the pressure that this vapor generates [33,39]. However, the total pressure on the atmosphere is the sum of the pressure caused by dry air plus the pressure produced by water vapor [8,40]. Thus, the greatest vapor pressure that may be present depends of the surface temperature [41]. As the temperature increases, more vapor pressure can be contained in the air [42,43]. This can be expressed by the Clausius–Clapeyron relationship [44,45].

Therefore, when the air is saturated with water vapor, the pressure of the water vapor depends only on the temperature [46]. On the other hand, the temperature of moist updrafts initialized at the surface and the greatest cloud depth are clear functions of surface dewpoint [34]. Consequently, a simple model should be proposed that carries the relationship (proportion) between pressure and dewpoint $\left(\frac{\partial P}{\partial T_d}\right)$. This model must also allow for confirmation of the key role of the surface humidity on convective activity. If it is accepted that meteorological parameters such as pressure, temperature, and relative humidity change at different altitudes [47], a synoptic evolution model crossing a series of humidity, dewpoint, and atmospheric pressure can be implemented.

2.2. The Proposed Model

The ARMA models (p,q) are the autoregressive AR models (p) to which an MA component (q) , called moving averages, has been added, and Box–Jenkins models are formed. The general type of the model is $Z_t = \sum_{j=1}^p \alpha_j Z_{t-j} + \varepsilon_t$ where p is the order of the autoregressive model; Z_t is the standardized variable in time t ; ε_t is the residual series; and α_j is the autoregressive coefficient. To estimate the parameters $\alpha_1, \alpha_2, \dots, \alpha_p$ the system of p nonlinear equations is resolved using the autocovariance function $r_k = \hat{\alpha}_j r_{k-1} + \hat{\alpha}_j r_{k-2} + \dots + \hat{\alpha}_p r_{k-p}$, $k > 0$. The parameters α_j are obtained by $\hat{\alpha}_j$.

To construct the proposed model called CRHUDA, there are two independent time series ($S1 \subseteq S2$) of climatic variables $S1$ and $S2$ defined by an autoregressive model of first-order AR(1):

$$S1 = H_t = \phi_1 H_{t-1} + \varepsilon_t \text{ and } S2 = C_t = \varphi_1 C_{t-1} + \varepsilon_t \quad (4)$$

where $\phi_1 = r_1$ and $\varphi_1 = r_1$ are the serial autocorrelation lag coefficients in time $k = 1$ for each of the series. This means that there is a proportionality coefficient in both series that allows the series to be scaled to cross in time t_1 . However, it should be remembered that the lag autocorrelation coefficient in time $k = 0$, is equal to 1.

The C in Equation (3) is replaced with the value of atmospheric pressure (P), and in the denominator, (T) is replaced with the dewpoint temperature (T_d), similar to [48]. In this way, two different time series are plotted: the first one is the humidity ($S1$) data and the second one is series ($S2$), defined by $\left(\frac{\partial P}{\partial T_d}\right)$, similar to the Clausius–Clapeyron relation. The crossing of these two series will show at the beginning of the alert ($t_1 : S1 \subseteq S2$), and some hours later, the series T_t will again cross ($t_2 : S1 \cap S2$) and, at that moment, precipitation will start $T_t + \Delta t$. Figure 1 shows the conceptual scheme of the model CRHUDA model. If the model predicts the exact start of precipitation, then $\Delta t \rightarrow 0$.

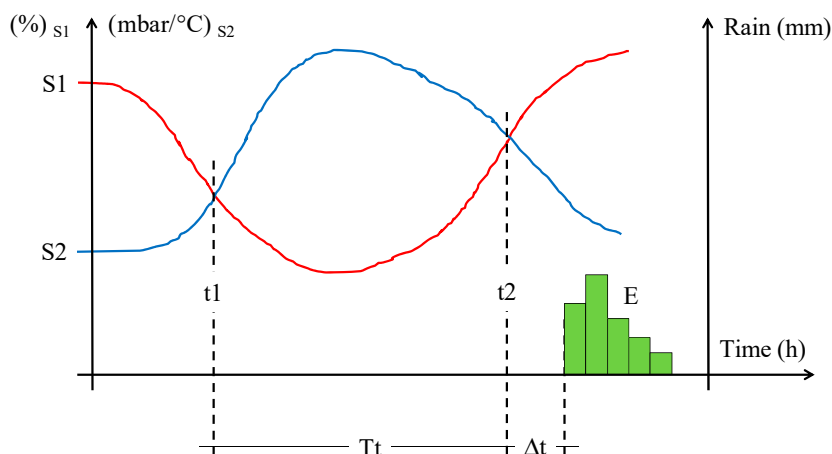


Figure 1. Conceptual scheme of the model CRHUDA (CRossingHUmidity, Dewpoint, and Atmospheric pressure).

$$CRHUDA (S1 \subseteq S2) \rightarrow (S1 \cap S2) \begin{cases} S1 = \text{humidity} \\ S2 = \frac{\Delta P}{\Delta T} = \frac{\partial P}{\partial T_d} = \frac{\text{atmospheric pressure}}{\text{dewpoint}} \end{cases}$$

This means that for the precipitation to begin, it must happen on $t1$ $H_{t1} = C_{t1}$; $(S1 \cap S2)$, and that considering $T_t + \Delta t$, $H_{t2} = C_{t2}$ at $t2$. If $\Delta t = 0$, the forecast of the start of the precipitation event E is precise. If $\Delta t \neq 0$, there is a time delay in the start of the precipitation event E .

2.3. The Precipitation Network RedCIAQ

In the city of Queretaro, in the middle of the Mexican republic, there is a network of 34 weather stations distributed all over the territory of the State and almost 34 stations concentrated in the capital city of Queretaro’s Extreme Precipitation Monitoring Network (RedCIAQ). The collection of data is done minute by minute and in real time such that there is a database of more than 20 million datasets available [24,49]. This climate monitoring network is one of the most advanced systems in Latin America and the Caribbean, and more than 18 hydroinformatics tools have also been developed to allow several analyses to be carried out in real time [50].

The variables monitored by the sensors installed in the automatic meteorological stations (EMA) are rainfall temperature, wind speed and direction, solar radiation, dewpoint, humidity, and atmospheric pressure all transmitted in real time in the portal web (redciaq.uaq.mx) and are extensively consulted by citizens and academic and scientific societies of the state in addition to the municipal and state authorities for the implementation of alerts and support programs for vulnerable sectors. Figure 2 shows the monitoring screen of one of the RedCIAQ stations. When a station is selected, its weather variables are displayed in real time, with a graph of the last 24 h. Figure 3 shows the location of the EMA within the Mexican territory. The real-time details of these stations can be consulted at <https://smn.conagua.gob.mx/es/pronosticos/8-smn-general/38-estaciones-meteorologicas-automaticas-emas>. Appendix A shows the details of the location of these stations. With the data of 523 storms registered from 2012 to 2018, we obtained the time series for the climatic variables of precipitation, humidity, atmospheric pressure, and dewpoint.

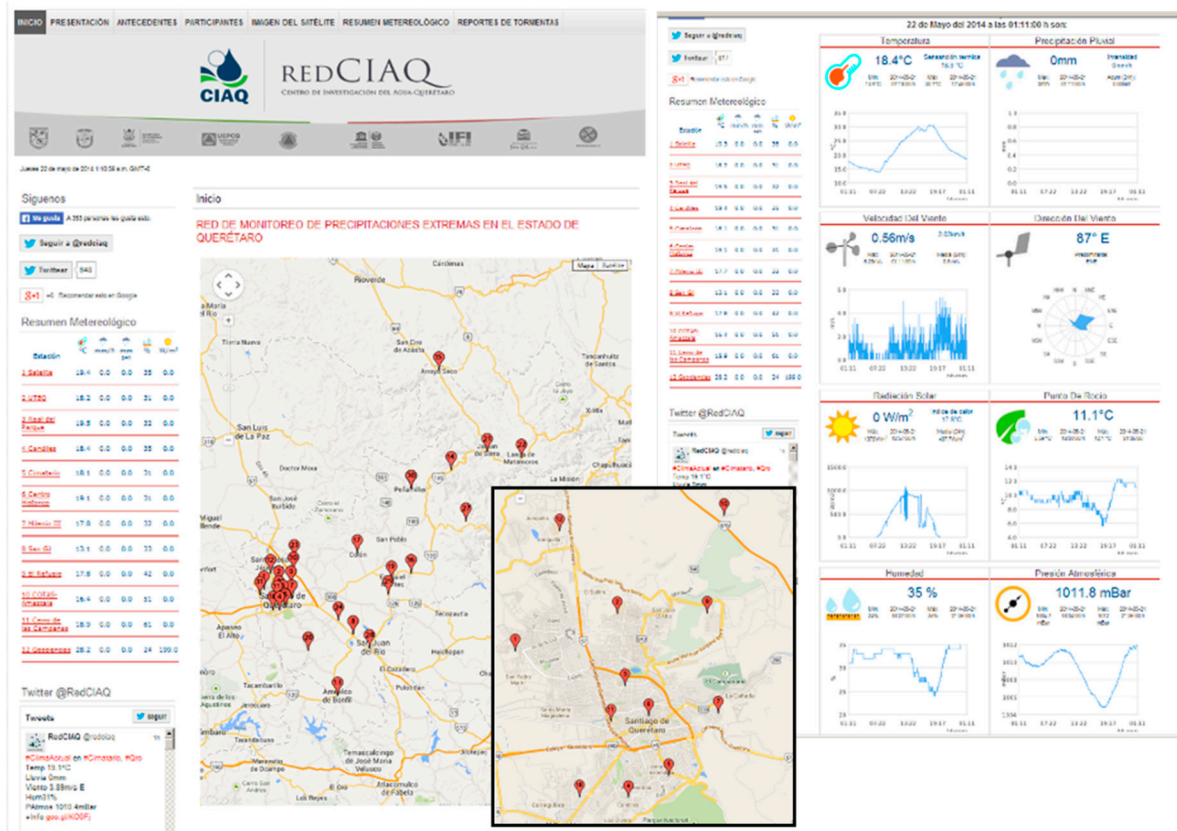


Figure 2. Queretaro’s Extreme Precipitation Monitoring Network real-time transmission website.

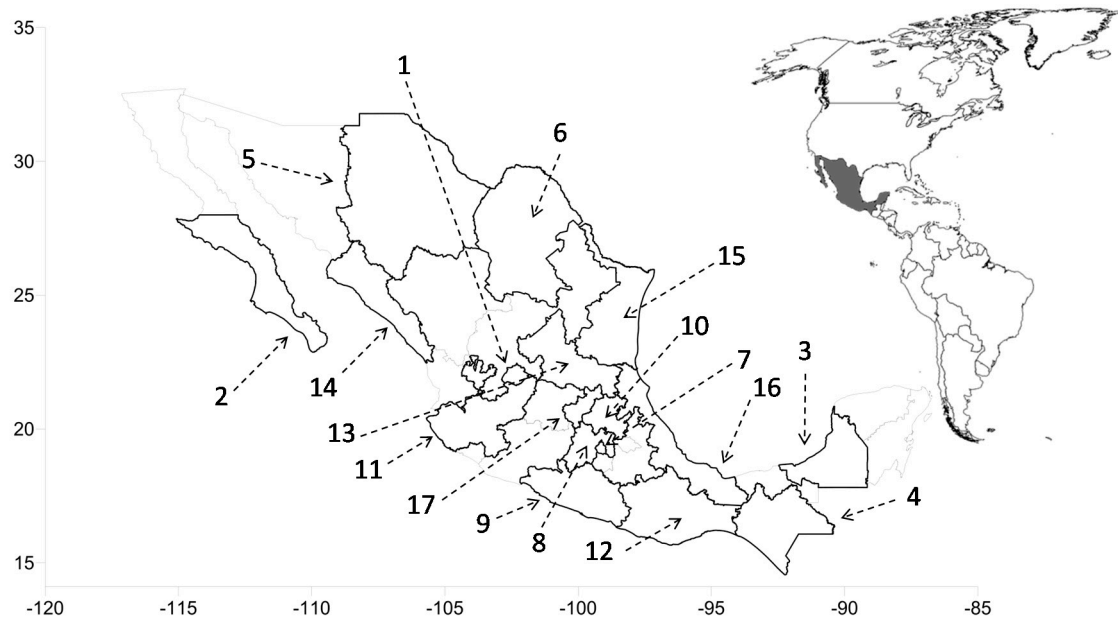


Figure 3. Location of each automatic meteorological station (EMA) and the number of storms by state. The numbers of states are shown in Table 1.

Figure 4 shows an example of time series obtained from pressure and temperature data. In Figure 4, it can be seen that there is a cross relation between these two time series. This same phenomenon is documented in some works when saturation pressure and temperature time series are used. Although there is precipitation, this was not detected in the series of atmospheric pressure and humidity, so it is

necessary to add other climate variables. Figure 5 shows the time series obtained from the data of pressure and humidity at the same time as the occurrence of the precipitation. In this time series, it can be observed that both series are almost parallel over time. Although there are two different phenomena at different scales, the behavior is very important to maintain continuity of the phenomenon. Once this same behavior has been verified in all datasets for all storms at all EMA stations, the CRHUDA ratio is obtained and the results are plotted.

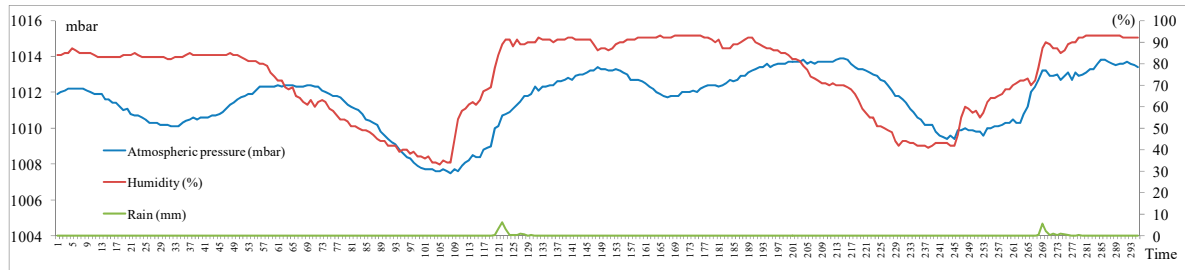


Figure 4. Example of the time series obtained from the data of pressure and humidity in the same time as the occurrence of the precipitation.

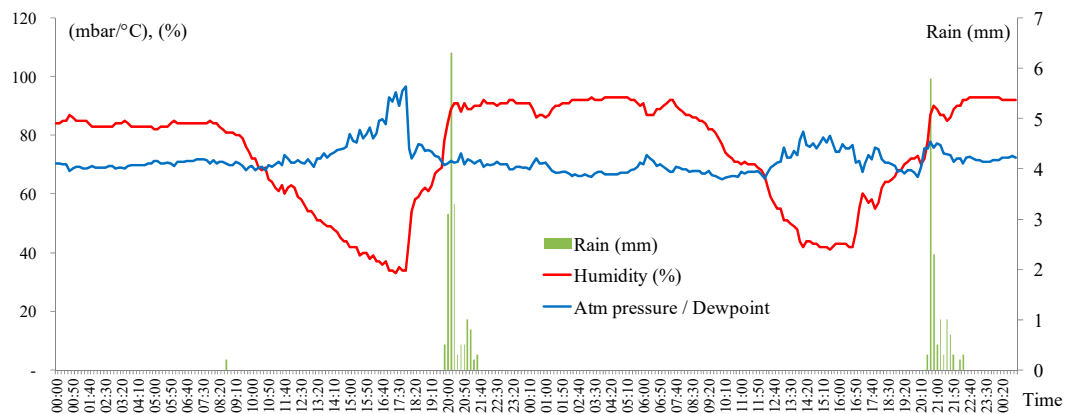


Figure 5. Results of applying the CRHUDA model at the automatic meteorological station Candiles on June 24–25, 2013.

3. Results

To set up a precise prediction model for precipitation, we used the CRHUDA model (Equation (4)) and applied three meteorological variables: 1) humidity, 2) dewpoint, 3) atmospheric pressure [3,51]. These three main variables have been shown to be linked with each other; when used in a crossover model of climate variables, the onset of a storm can be predicted [37,52]. As a consequence, boundaries for each variable should be individually established first, and analyzed afterwards to determine how they are able to relate with each other to obtain a response in a proper scenario [53,54].

The procedure consists of the time series being available at each minute for the three climatic variables referred above. Minute by minute, both series are distributed parallel on the time axis. In a synoptic sense, it is possible to see, surprisingly, that the crossing of these two time series generates a point in time that allows generating an alert between 9 and 10 h in advance of the start of the storm, at about 10:20 in Figure 5. After the first crossing, when the humidity drops quickly, these series cross one more time but in the opposite direction to the start of the precipitation. This procedure was carried out with data from the historical records of the 34 stations of the Queretaro State Extreme Precipitation Monitoring Network (RedCIAQ). During the seven years of minute-by-minute records, the variables used by CRHUDA were measured, then 523 convective events were identified. The calibration of the model was carried out with these 523 storms. To confirm the model, it was necessary to apply it to the data that were monitored every minute, and then apply it to the EMA stations of the

Mexican territory, which take data every 20 min. The calibration results showed a mean time of 10 h ($T_t + \Delta t = 619.58$ min) between the t_1 alert and the start of precipitation t_2 , with a median of 8.9 h (535 min). The calibration results also showed that the scale factor for the humidity series varied between 0.4 and 2.6 with a mean of 1.784 and a median of 1.84 and, as discussed, the mode was equal to 1. This means that there is, in fact, a stochastic behavior in the time series.

Due to large amount of data that was analyzed, a hydroinformatics tool was created that allows the systematic analysis of all EMA records in the Mexican territory. The tool is called CRHUDA, and is copyrighted. It was developed in C+ language and current work on a second version includes forecasting with ARMA(p,q) models. Some of the Caribbean countries have begun to provide information to verify the usefulness of the proposed model in other regions. Figure 5 shows the results of applying the CRHUDA model at the automatic meteorological station Candiles on June 24–25, 2013. Two storms can be observed, which are then divided into Figures 6 and 7 for detailed analysis.

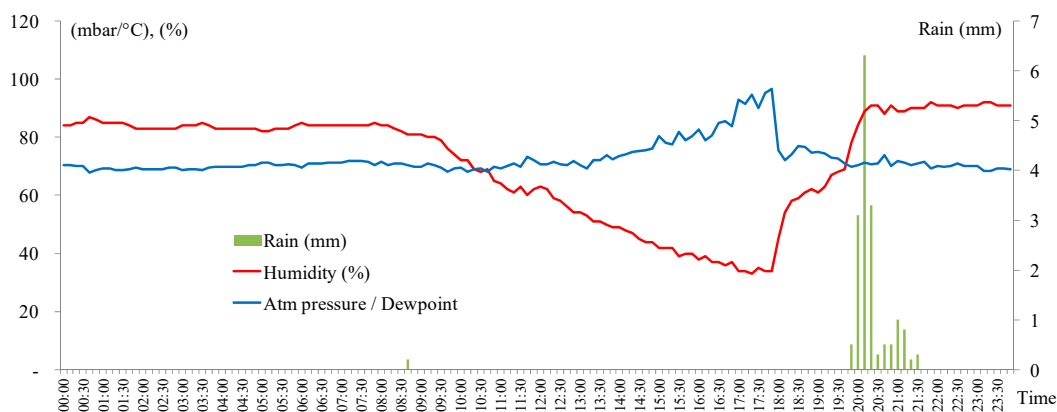


Figure 6. Results of applying the CRHUDA model at the automatic meteorological station Candiles on June 24, 2013.

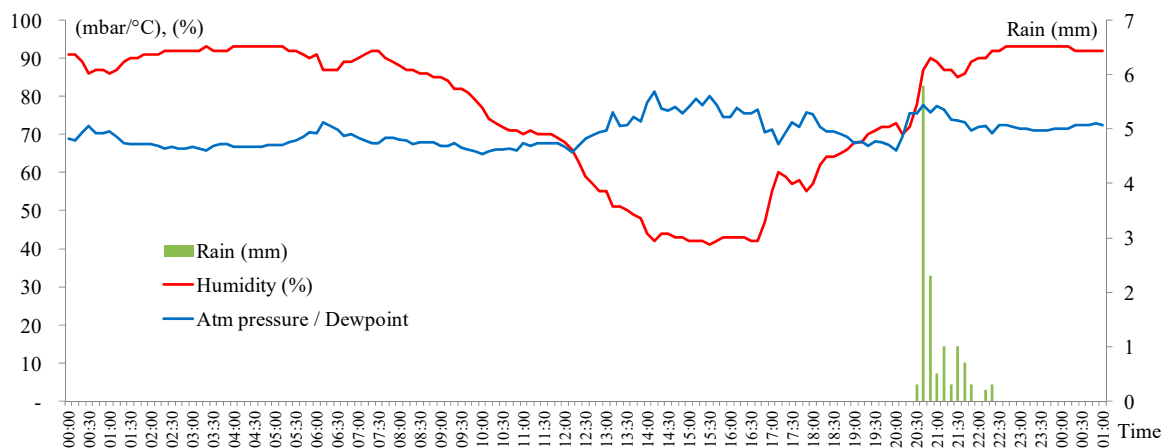


Figure 7. Results of applying the CRHUDA model at the automatic meteorological station Candiles on June 25, 2013.

Tables 1 and 2 show the values of the climatic variables used in the CRHUDA model for time t_1 (warning) and t_2 (start of precipitation), respectively, at the EMA Candiles on June 24, 2013.

Table 1. Climatological values at time t1 $H_{t1} = C_{t1}; (S1 \cap S2)$ at EMA Candiles on June 24, 2013.

Date	Time	Humidity (%)	Atm Pressure/Dewpoint
24/06/2013	09:50	74	69.240
24/06/2013	10:00	72	69.447
24/06/2013	10:10	72	68.095
24/06/2013	10:20	69	68.961
24/06/2013	10:30	68	69.134
24/06/2013	10:40	69	68.076
24/06/2013	10:50	65	69.758
24/06/2013	11:00	64	69.105

Table 2. Climatological values at time t2 $H_{t2} = C_{t2}$ at EMA Candiles on June 24, 2013.

Date	Time	Humidity (%)	Atm Pressure/Dewpoint	Rain (mm)
24/06/2013	19:00	61	75.069	0
24/06/2013	19:10	63	74.398	0
24/06/2013	19:20	67	72.876	0
24/06/2013	19:30	68	72.679	0
24/06/2013	19:40	69	71.039	0
24/06/2013	19:50	78	69.783	0.5
24/06/2013	20:00	84	70.342	3.1
24/06/2013	20:10	89	71.287	6.3
24/06/2013	20:20	91	70.559	3.3
24/06/2013	20:30	91	71.056	0.3
24/06/2013	20:40	88	73.763	0.5
24/06/2013	20:50	91	70.110	0.5
24/06/2013	21:00	89	71.843	1
24/06/2013	21:10	89	71.365	0.8
24/06/2013	21:20	90	70.502	0.2
24/06/2013	21:30	90	70.997	0.3
24/06/2013	21:40	90	71.520	0

Figures 8–11 show an example of the results after applying the CRHUDA model to the historical data series of the most representative stations of the RedCIAQ. The figures show the model application to convective storm data. For the storms, the total rainfall depth and the return period corresponding to storm duration are provided.

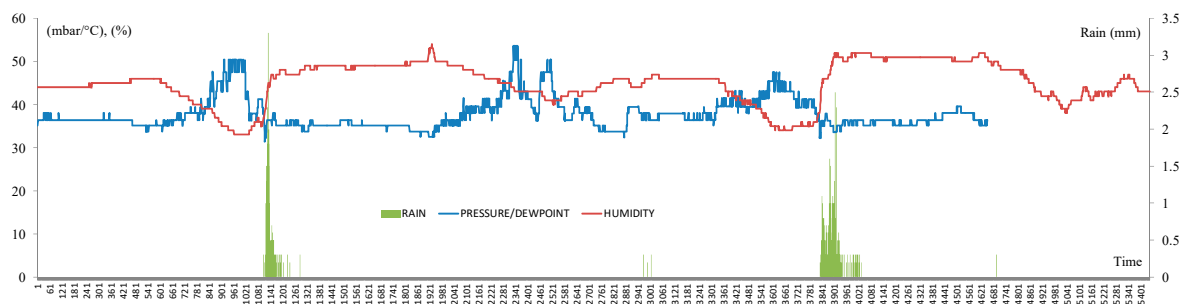


Figure 8. Results of applying the CRHUDA model to Centro Historico data on August 16, 2014 (max depth 10.9 mm in 1 h; max intensity 24.3 mm/h; 17-year return period).

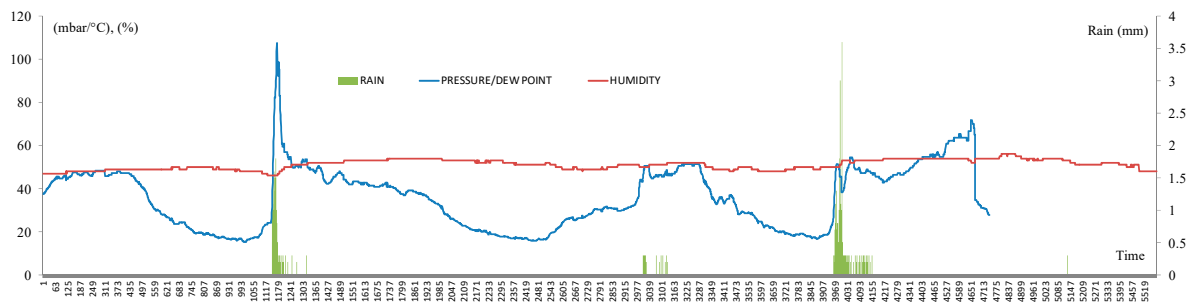


Figure 9. Results of applying the CRHUDA model to Cimatario data on August 16, 2014 (max depth 15.4 mm in 1 h; max intensity 41.2 mm/h; 32-year return period).

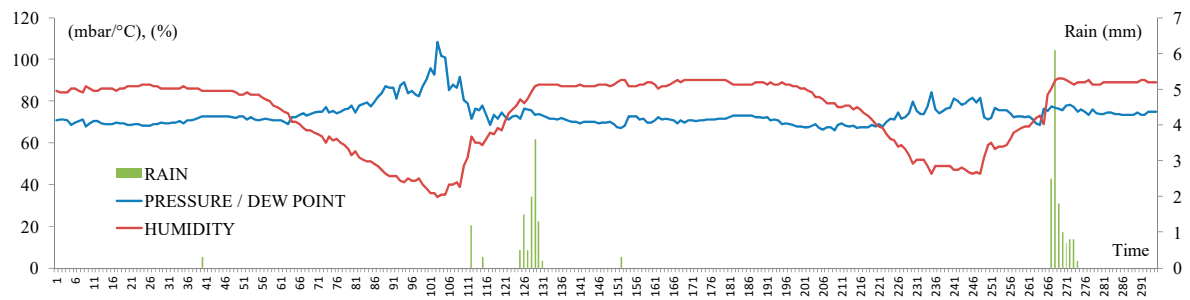


Figure 10. Results of applying the CRHUDA model to Milenio data on August 16, 2014 (max depth 12.1 mm in 1 h; max intensity 42.3 mm/h; 37-year return period).



Figure 11. Results of applying the CRHUDA model to UAQ Cerro Campanas data on August 16, 2014 (max depth 55.2 mm in 1 h; max intensity 63.8 mm/h; 53-year return period).

In order to validate the CRHUDA model throughout the territory of Mexico, the model was executed in the same way as 17 out of the 32 states of Mexico. Figures 12–15 show the results of the crossing between the humidity, dewpoint, and atmospheric pressure model. In addition to the 523 storms analyzed in Queretaro, a total of 714 storms were analyzed in 16 Mexican states. Table 3 shows the number of storms and the names of the EMA stations used in each state. Thus, the total number of events analyzed was 1237 convective storms between 1999 and 2018. This database also includes storms caused by hurricanes.

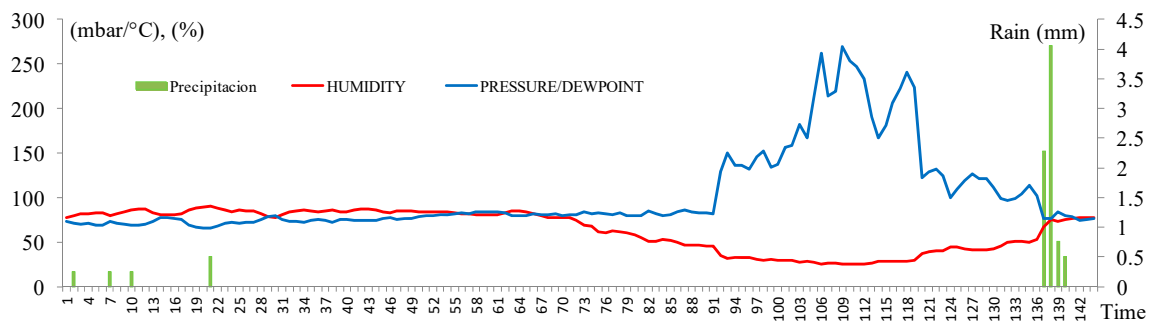


Figure 12. Results of applying the CRHUDA model to Atlacomulco data on April 23, 2018.

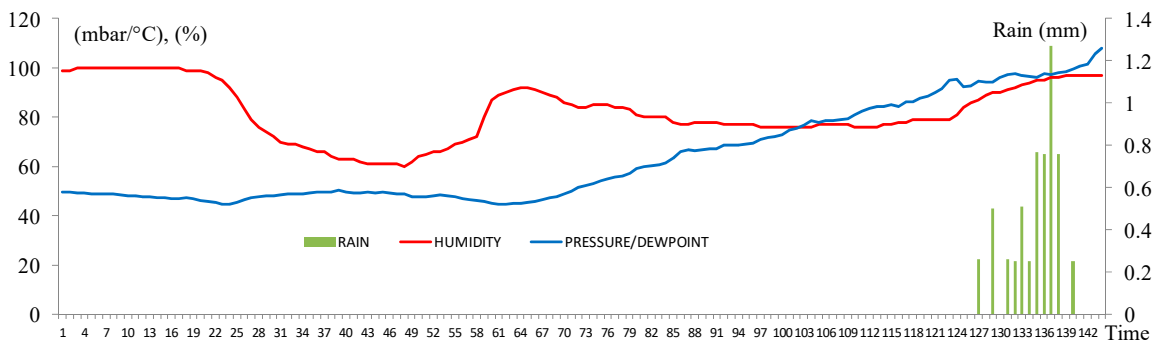


Figure 13. Results of applying the CRHUDA model to B. Del Tordo data on November 12, 2018.

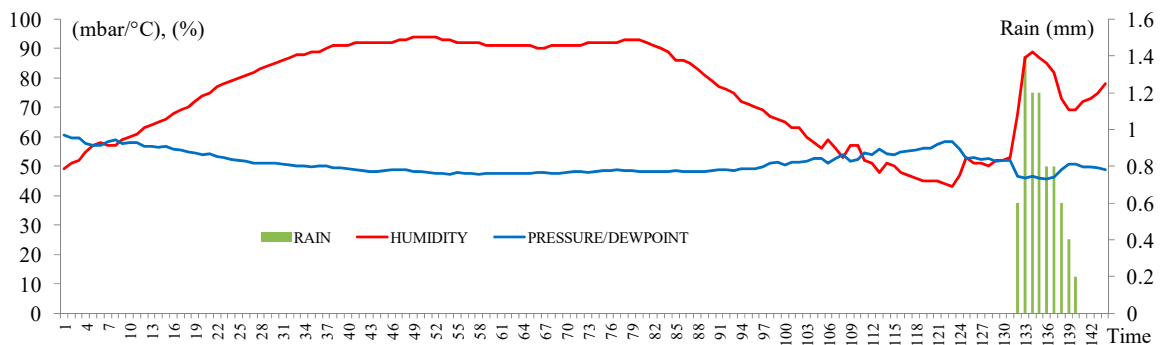


Figure 14. Results of applying the CRHUDA model to Dzilbachen data on February 22, 2018.

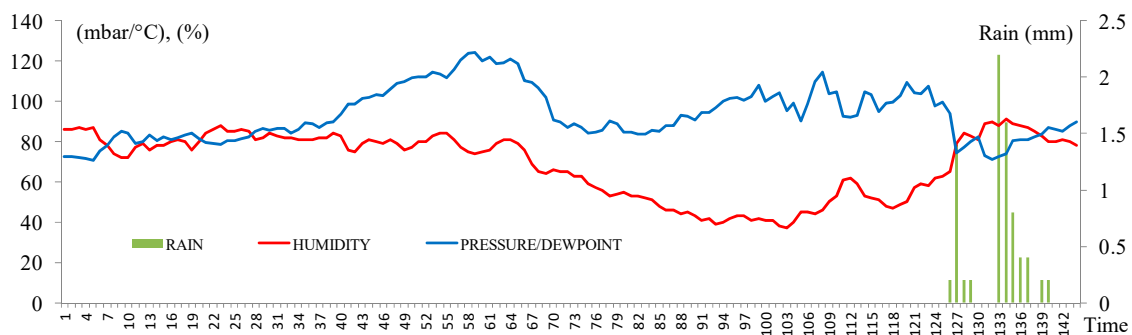


Figure 15. Results of applying the CRHUDA model to Ecoguardas data on April 6, 2018.

Table 3. Location of each automatic meteorological station (EMA) and the number of storms by state.

	State ID	Storms	EMA's Name
1	Aguascalientes	47	Calvillo
2	Baja California Sur	6	Cabo San Lucas
3	Campeche	12	Dzilbachen
4	Chiapas	85	El Triunfo
5	Chihuahua	48	Basaseachic
6	Coahuila	19	Cuatro Cienegas
7	DF	76	Ecoguardas
8	Edo. de Mexico	160	Atlacomulco, Cerro Catedral
9	Guerrero	1	Ciudad Altamirano
10	Hidalgo	51	El Chico
11	Jalisco	18	Chamela-Cuixmala
12	Oaxaca	41	Benito Juarez
13	San Luis Potosi	35	Ciudad Fernandez, Ciudad Valle
14	Sinaloa	24	El Fuerte
15	Tamaulipas	32	B. Del Tordo
16	Veracruz	59	Ciudad Aleman, Coscomatepec
	Subtotal	714	
17	Queretaro	523	See Appendix A, for details (34 EMA)
	Total	1237	

4. Discussion

A strong relationship between surface temperature and precipitation forecast has been reported in the literature, in addition to how these climatic variables impact streamflow ensemble forecasting [55]. According to [56], the potential for rainfall forecasts to be used in hydrological models to predict river flow depends on the response of the basin to earlier events and on the timing of the present event. The question is: What is the forecast time of rainy events? One implication of this is the possibility that a good rainfall forecasting model could be used in an early warning system for floods. Prior studies have noted the importance of short time scales, and that more extreme precipitation is more sensitive to temperature changes. Understanding how precipitation characteristics change in response to climatic elements provides new insight into convective organization and the structure of short-duration storms [33]. The present study was designed to find the effect of the Clausius–Clapeyron relationship and combination of atmospheric pressure, dewpoint, and humidity as the variables that cause most meteorological phenomena, in particular, precipitation. The results of this study show that it is possible to combine the climatic variables mentioned in two series that can be synoptically plotted to determine where both series cross, and this usually occurs, on average, between 9 and 10 h before the start of precipitation. It can therefore be assumed that the CRHUDA model includes the C–C relationship and, additionally, it allows combining of the aforementioned variables into a simple model for forecasting the onset of precipitation. These results are consistent with those of other studies that suggest that the dependency on surface dewpoint temperature follows two times the C–C relation, supported by the simple physical argument that this 2C–C behavior arises from the physics of convective clouds [34]. It is somewhat surprising that CRHUDA, as a simple synoptic model, can predict the onset of precipitation in a trustworthy way. Between 9 and 10 h beforehand, the forecast seems acceptable; this is also in accordance with our earlier observations which showed that it is possible to use the minute-by-minute hydrometeorological real-time dataset. Hence, it can be suggested that a daily rainfall database allows the correct spatial–temporal disaggregation in spatially distributed hourly rainfall [57]. Although these results differ from some published studies [58], models such as GEFSRv2 and SREF tend to overforecast light to moderate precipitation and underforecast heavy precipitation. Hence, a rainfall disaggregation model to which the temperature has been added as a driver should offer a more realistic assessment of future precipitation extremes [59]. According to [35], in a graph of rain intensity versus temperature, the crossover point between the two series always occurs at the onset of precipitation. This finding

has important implications for the development of a precipitation forecasting model for providing forecasts 9–10 h in advance, as it is only necessary to find the right combination of climate variables. Therefore, the results of the CRHUDA model suggest its applicability in the Mexican territory.

In most cases, the start of precipitation was precise. In other words, in almost all cases, $\Delta t = 0$. Although there are some events that anticipated crossings and a delay in precipitation starting point happened as shown in Figures 13 and 14, the proposed model is able to provide estimates between 9 and 10 h in advance. Figure 16 shows the frequency histogram of the warning times for Queretaro stations in 2018. Figure 17 shows the frequency histogram of the proportionality coefficient ϕ_1 for all of the Queretaro EMAs in 2018.

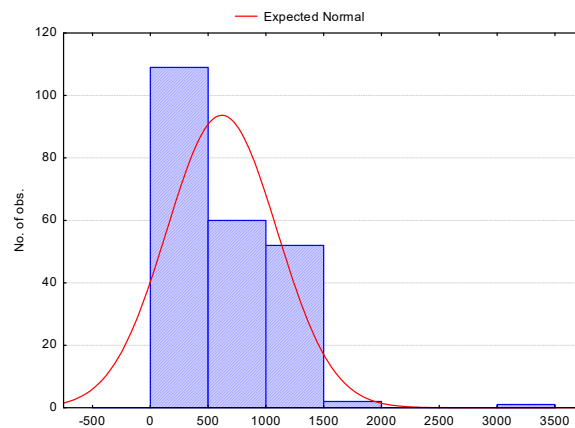


Figure 16. Frequency histogram of the warning times (in minutes) $T_t + \Delta t$ for all of the Queretaro EMAs in 2018.

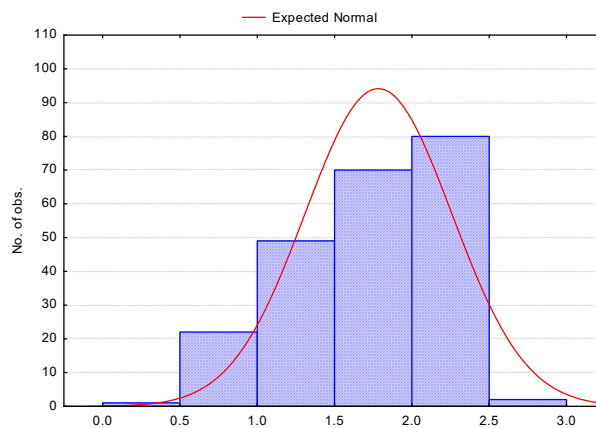


Figure 17. Frequency histogram of proportionality coefficient ϕ_1 for all of the Queretaro EMAs in 2018.

Regarding the proportionality coefficient or the parameter of an AR(1) model, it is important to mention that these coefficients were obtained in all cases. However, the hydroinformatics tool works, by default, with a value equal to 1. This is because it was shown that the coefficient of the AR(1) model only allows moving the humidity series within the graph, as shown in Figure 18.

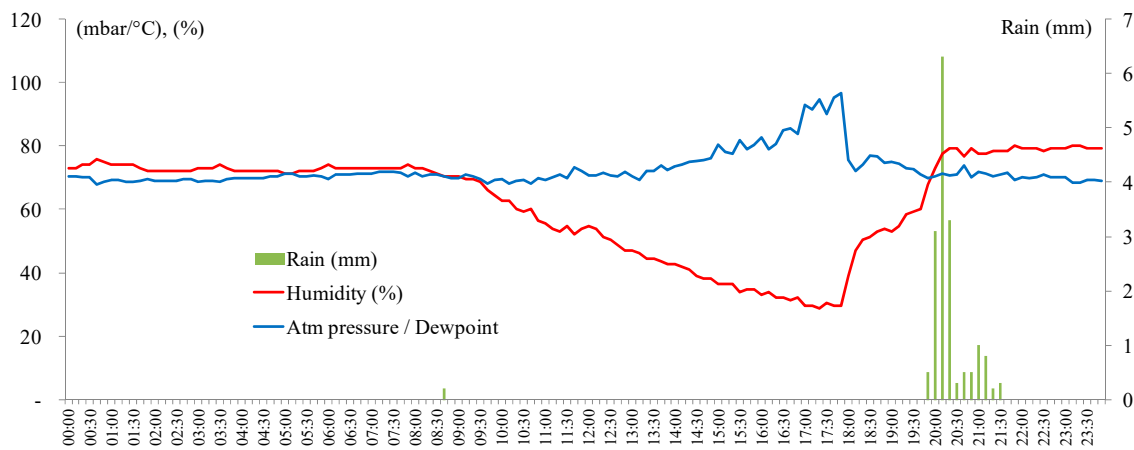


Figure 18. Results of applying the CRHUDA model at the automatic meteorological station Candiles on June 24, 2013 with $r_1 = 0.8746$.

It is interesting to compare Figures 6 and 18, since they concern the same EMA station during the same storm, but the parameter of the AR(1) model has been included. It is observed that the values of forecast time and precipitation occurrence do not vary. However, when scaling the series, the crossing time is clearer. This procedure is carried out in real time on days when the crossing of series is not clear. That is to say, for greater precision, the stochastic parameters of the time series are used.

To finish in terms of propositional logic, the truth table construction is shown below (Table 4). It starts with the two main premises: If there is a crossing of the two proposed series in time ($t1 : S1 \subseteq S2$) then, some hours later, the T_t series will cross again ($t2 : S1 \cap S2$) and, at that moment, $T_t + \Delta t$, precipitation will begin. If there is no crossing, then there will be no rain.

Table 4. Propositional logic truth table of the CRHUDA model.

$S1 \subseteq S2$	$S1 \cap S2$	$(S1 \subseteq S2) \rightarrow (S1 \cap S2)$	$\sim(S1 \subseteq S2) \rightarrow \sim(S1 \cap S2)$	$(S1 \subseteq S2) \rightarrow (S1 \cap S2) \wedge \dots$ $\dots \sim(S1 \subseteq S2) \rightarrow \sim(S1 \cap S2)$
True	True	True	True	True
True	False	False	True	False
False	True	True	False	False
False	False	True	True	True

It is concluded that it is, in fact, a valid model of the type contingency; a compound proposition which is sometimes true and sometimes false. That is to say, contingent truth, or truth, in fact, is understood as that proposition that can be true or false, according to the values of its constituent propositions.

5. Conclusions

Mexico’s National Center for Disaster Prevention establishes that one of the mechanisms used by the Mexican government to protect against and mitigate damage caused by disasters of different types is an early warning system. To guarantee its proper functioning, the coordinated participation of scientific groups, technical agencies, those responsible for communication and dissemination, as well as the population itself is required. The National Center for Disaster Prevention emphasizes warnings: “you must keep in mind that a clear and timely warning, along with knowledge of what is expected and how to react, makes a great difference for people and their communities”. Therefore, it is essential to inform the population in an accessible way and in sufficient time to mitigate the effects of natural phenomena [60]. The proposed model is a simple model that can surprisingly predict the starting point of precipitation 9–10 h in advance.

This paper has highlighted the relevance of having a simple forecast precipitation model and the reasons for the widespread use Clausius–Clapeyron relation. This paper has argued that a combination of crossing humidity, dewpoint, and atmospheric pressure is the best instrument for making a synoptic forecast of precipitation onset. Two sets of series were considered: (i) humidity and (ii) the relationships between atmospheric pressure and dewpoint. This phenomenon of crossing variables was verified through the analysis of 1237 storms. Recent studies show that the time series of temperature and humidity, when properly combined, can generate a trusted precipitation forecasting model [61].

Taken together, these results suggest that current early warning systems could be based on measurements of rainfall intensity. Those systems could be combined with monitoring of water levels [62,63]. These findings suggest several courses of action to record, send, and monitor floods using a new generation of smart water level gauges [64]. Another important practical implication is, for example, as occurred in Tabasco, Mexico, that the climatic information from a flood early warning system is transmitted in real time and published using a social network (Twitter) by radio frequency (915 MHz) using LoRa modulation [65]. An implication of this is the possibility that in the LAC region, a simple extreme rainfall warning system can be implemented at low cost, due to the fact that the application of the CRHUDA model only requires three measured climatic variables. To date, only precipitation forecast models based on the principle of analogue prediction are capable of producing accurate forecasts with a 6 to 8 h lead time in forecasting [59]. Currently, in other countries, the simple implementation of extreme rainfall warning systems combined with flood simulation models is a priority. Many developing countries are working to cut the number of fatalities due to flash floods, improve the efficiency of disaster risk reduction efforts, and play an important role in strengthening the resilience to climate change [66]. In these cases, CRHUDA could be an algorithm that is easy to implement.

At present, we are working on characterizing the spatial–temporal relationship of the parameters of the AR(1) models in the used climatological series. It is expected that it will soon be possible to demonstrate that the parameters of these AR(1) models vary with some differences in spatial patterns in the Mexican territory. For now, it was important to present the model and its application to other regions.

Returning to the suggestion posed at the beginning of this study, we presented a simple forecasting model for precipitation onset based on crossing humidity, dewpoint, and atmospheric pressure. Therefore, there is a definite need to continue research into estimating the uncertainty of precipitation onset and many further improvements are required, including the inputs of EWS [67]. The CRHUDA model was already tested during the current rainy season (2019), achieving great precision in forecasting the start of precipitation. The authors invite researchers to apply the CRHUDA model to their time series to validate this forecasting model.

Author Contributions: Conceptualization, formal analysis, methodology and validation A.G.-L.; software, data curation, and writing—original draft preparation, I.C.-P. M.M.M. contributed to the systematization of the calculations of the model CRHUDA, resources, software.

Funding: This research received funding of Secretaria de Educacion Publica (SEP-Mexico). Programa para el Desarrollo Profesional Docente (PRODEP) and was supported by the Fund for the Reinforcement of Research UAQ-2018 Research and Postgraduate Division (FOFIUAQ/FIN201911).

Acknowledgments: The authors are grateful to the Risk Management Unit of the UNESCO Regional Office of Science for Latin America and the Caribbean. We express our sincere gratitude to Josue Elizondo Gomez, Miguel Angel Sanchez Quijano and Bruno Miguel Paz Aviña for discussions on the topic of this work. We acknowledge the constructive comments of the three anonymous reviewers.

Conflicts of Interest: The authors declare no conflict of interest.

Appendix A

Table A1. RedCIAQ Weather Stations.

Id	Name	Long	Lat	Id	Name	Long	Lat
1	Chulavista	−100.47	20.63	18	Ezequiel Montes	−99.90	20.67
2	Belén	−100.41	20.65	19	Huimilpan	−100.27	20.37
3	Real del Parque	−100.40	20.61	20	Landa de Matamoros	−99.32	21.18
4	Candiles	−100.40	20.55	21	Pedro Escobedo	−100.14	20.50
5	Cimatario	−100.38	20.56	22	San Joaquín	−100.01	20.38
6	Centro histórico	−100.39	20.59	23	San Juan del Rio	−99.97	20.39
7	Milenio III	−100.35	20.59	24	Tequisquiapan	−99.91	20.61
8	San gil	−100.44	20.70	25	Toliman	−99.93	20.90
9	El refugio	−100.35	20.65	26	Viñedos	−100.49	20.61
10	COTAS Amazcala	−100.34	20.71	27	El esparrago	−100.01	20.38
11	Cerro de las Campanas	−100.41	20.59	28	Santa Rosa Jáuregui	−100.45	20.74
12	Amealco de Bonfil	−100.14	20.19	29	Unión de Ejidos	−100.23	20.65
13	Pinal de Amoles	−99.63	21.14	30	Joaquín Herrera	−99.57	20.92
14	Arroyo seco	−99.69	21.55	31	Juriquilla	−100.45	20.72
15	Cadereyta de Montes	−99.81	20.70	32	UAQ Aeropuerto	−100.37	20.62
16	Colon	−100.05	20.78	33	Pasteur y 57	−100.38	20.58
17	Corregidora	−100.43	20.55	34	CICATA QRO IPN	−100.37	20.57

References

1. CENAPRED. *Disasters in Mexico: Social and Economic Impacts (1980–2014)*; Centro Nacional de Prevención de Desastres: Secretaría de Gobernación, Mexico, 2016.
2. Gutierrez-Lopez, A.; Fortanell Trejo, M.; Albuquerque Gonzalez, N.; Bravo Prado, F. Análisis de la variabilidad espacial en la precipitación en la zona metropolitana de Querétaro empleando ecuaciones de anisotropía. In *Investigaciones Geográficas*; Instituto de Geografía, Universidad Autónoma de México: Ciudad de México, Mexico, 2019. [\[CrossRef\]](#)
3. Lepore, C.; Allen, J.; Tippet, M. Relationships between Hourly Rainfall Intensity and Atmospheric Variables over the Contiguous United States. *J. Clim.* **2016**, *29*, 3181–3197. [\[CrossRef\]](#)
4. Saltzman, B. On the Maintenance of the Large-Scale Quasi-Permanent Disturbances in the Atmosphere. *Tellus* **1959**, *11*, 425–431. [\[CrossRef\]](#)
5. Saltzman, B. *Dynamical Paleoclimatology*, 1st ed.; Academic Press: New York, NY, USA, 2002.
6. Lorenz, E. Deterministic Nonperiodic Flow. *J. Atmos. Sci.* **1963**, *20*, 130–141. [\[CrossRef\]](#)
7. Berg, P.; Haerter, J. Unexpected increase in precipitation intensity with temperature—A result of mixing of precipitation types? *Atmos. Res.* **2013**, *119*, 56–61. [\[CrossRef\]](#)
8. Holley, D.; Dorling, S.; Steele, C.; Earl, N. A climatology of convective available potential energy in Great Britain. *Int. J. Climatol.* **2014**, *34*, 3811–3824. [\[CrossRef\]](#)
9. Lekouch, I.; Lekouch, K.; Muselli, M.; Mongruel, A.; Kabbachi, B.; Beysens, D. Rooftop dew, fog and rain collection in southwest Morocco and predictive dew modeling using neural networks. *J. Hydrol. (Amst.)* **2012**, *448*, 60–72. [\[CrossRef\]](#)
10. Park, I.; Min, S. Role of Convective Precipitation in the Relationship between Subdaily Extreme Precipitation and Temperature. *J. Clim.* **2017**, *30*, 9527–9537. [\[CrossRef\]](#)
11. Dyson, L.; van Heerden, J.; Sumner, P. A baseline climatology of sounding-derived parameters associated with heavy rainfall over Gauteng, South Africa. *Int. J. Climatol.* **2014**, *35*, 114–127. [\[CrossRef\]](#)
12. Omotosho, J. Equivalent potential temperature and dust haze forecasting at Kano, Nigeria. *Atmos. Res.* **1989**, *23*, 163–178. [\[CrossRef\]](#)
13. Puvaneswaran, M. Climatic classification for queensland using multivariate statistical techniques. *Int. J. Climatol.* **1990**, *10*, 591–608. [\[CrossRef\]](#)
14. Damrath, U.; Doms, G.; Frühwald, D.; Heise, E.; Richter, B.; Steppeler, J. Operational quantitative precipitation forecasting at the German Weather Service. *J. Hydrol. (Amst.)* **2000**, *239*, 260–285. [\[CrossRef\]](#)
15. Rasouli, K.; Hsieh, W.; Cannon, A. Daily streamflow forecasting by machine learning methods with weather and climate inputs. *J. Hydrol. (Amst.)* **2012**, *414*, 284–293. [\[CrossRef\]](#)

16. Moon, S.; Kim, Y.; Lee, Y.; Moon, B. Application of machine learning to an early warning system for very short-term heavy rainfall. *J. Hydrol. (Amst.)* **2019**, *568*, 1042–1054. [[CrossRef](#)]
17. Zahraei, A.; Hsu, K.; Sorooshian, S.; Gourley, J.; Hong, Y.; Behrangi, A. Short-term quantitative precipitation forecasting using an object-based approach. *J. Hydrol. (Amst.)* **2013**, *483*, 1–15. [[CrossRef](#)]
18. Li, P.; Lai, E. Short-range quantitative precipitation forecasting in Hong Kong. *J. Hydrol. (Amst.)* **2004**, *288*, 189–209. [[CrossRef](#)]
19. Carrera-Hernández, J.; Gaskin, S. Spatio temporal analysis of daily precipitation and temperature in the Basin of Mexico. *J. Hydrol. (Amst.)* **2007**, *336*, 231–249. [[CrossRef](#)]
20. Carter, M.; Elsner, J.; Bennett, S. A quantitative precipitation forecast experiment for Puerto Rico. *J. Hydrol. (Amst.)* **2000**, *239*, 162–178. [[CrossRef](#)]
21. Valverde Ramírez, M.; de Campos Velho, H.; Ferreira, N. Artificial neural network technique for rainfall forecasting applied to the São Paulo region. *J. Hydrol. (Amst.)* **2005**, *301*, 146–162. [[CrossRef](#)]
22. Hou, T.; Kong, F.; Chen, X.; Lei, H. Impact of 3DVAR Data Assimilation on the Prediction of Heavy Rainfall over Southern China. *Adv. Meteorol.* **2013**, *2013*, 129642. [[CrossRef](#)]
23. Wang, J.; Gaffen, D. Late-Twentieth-Century Climatology and Trends of Surface Humidity and Temperature in China. *J. Clim.* **2001**, *14*, 2833–2845. [[CrossRef](#)]
24. Suparta, W.; Alhasa, K.; Singh, M. Estimation water vapor content using the mixing ratio method and validated with the ANFIS PWV model. *J. Phys. Conf. Ser.* **2017**, *852*, 012041. [[CrossRef](#)]
25. Camuffo, D. Theoretical Grounds for Humidity. In *Microclimate for Cultural Heritage*; Elsevier: Amsterdam, The Netherlands, 2014; Chapter 2A; pp. 49–76. ISBN 9780444632982. [[CrossRef](#)]
26. Pumo, D.; Carlino, G.; Blenkinsop, S.; Arnone, E.; Fowler, H.; Noto, L. Sensitivity of extreme rainfall to temperature in semi-arid Mediterranean regions. *Atmos. Res.* **2019**, *225*, 30–44. [[CrossRef](#)]
27. Capparelli, A. *Fisicoquímica Básica*, 1st ed.; Universidad Nacional La Plata Argentina: La Plata, Argentina, 2013.
28. Van der Dussen, J.; de Roode, S.; Siebesma, A. Factors Controlling Rapid Stratocumulus Cloud Thinning. *J. Atmos. Sci.* **2014**, *71*, 655–664. [[CrossRef](#)]
29. Romps, D. Clausius–Clapeyron Scaling of CAPE from Analytical Solutions to RCE. *J. Atmos. Sci.* **2016**, *73*, 3719–3737. [[CrossRef](#)]
30. Agard, V.; Emanuel, K. Clausius–Clapeyron Scaling of Peak CAPE in Continental Convective Storm Environments. *J. Atmos. Sci.* **2017**, *74*, 3043–3054. [[CrossRef](#)]
31. Lorenz, D.; DeWeaver, E. The Response of the Extratropical Hydrological Cycle to Global Warming. *J. Clim.* **2007**, *20*, 3470–3484. [[CrossRef](#)]
32. Romps, D. An Analytical Model for Tropical Relative Humidity. *J. Clim.* **2014**, *27*, 7432–7449. [[CrossRef](#)]
33. Chang, W.; Stein, M.; Wang, J.; Kotamarthi, V.; Moyer, E. Changes in Spatiotemporal Precipitation Patterns in Changing Climate Conditions. *J. Clim.* **2016**, *29*, 8355–8376. [[CrossRef](#)]
34. Lenderink, G.; Barbero, R.; Loriaux, J.; Fowler, H. Super-Clausius–Clapeyron Scaling of Extreme Hourly Convective Precipitation and Its Relation to Large-Scale Atmospheric Conditions. *J. Clim.* **2017**, *30*, 6037–6052. [[CrossRef](#)]
35. Bürger, G.; Heistermann, M.; Bronstert, A. Towards Subdaily Rainfall Disaggregation via Clausius–Clapeyron. *J. Hydrometeorol.* **2014**, *15*, 1303–1311. [[CrossRef](#)]
36. Peleg, N.; Marra, F.; Fatichi, S.; Molnar, P.; Morin, E.; Sharma, A.; Burlando, P. Intensification of Convective Rain Cells at Warmer Temperatures Observed from High-Resolution Weather Radar Data. *J. Hydrometeorol.* **2018**, *19*, 715–726. [[CrossRef](#)]
37. Velasco, S.; Fernández-Pineda, C. Sobre la obtención de la ecuación de Clapeyron–Clausius. *Rev. Española Física* **2008**, *22*, 7–14.
38. Seidel, T.; Grant, A.; Pszenny, A.; Allman, D. Dewpoint and Humidity Measurements and Trends at the Summit of Mount Washington, New Hampshire, 1935–2004. *J. Clim.* **2007**, *20*, 5629–5641. [[CrossRef](#)]
39. Millán, H.; Ghanbarian-Alavijeh, B.; García-Fornaris, I. Nonlinear dynamics of mean daily temperature and dewpoint time series at Babolsar, Iran, 1961–2005. *Atmos. Res.* **2010**, *98*, 89–101. [[CrossRef](#)]
40. Harder, P.; Pomeroy, J. Estimating precipitation phase using a psychrometric energy balance method. *Hydrol. Process.* **2013**, *27*, 1901–1914. [[CrossRef](#)]

41. Dahm, R.; Bhardwaj, A.; Sperna Weiland, F.; Corzo, G.; Bouwer, L. A Temperature-Scaling Approach for Projecting Changes in Short Duration Rainfall Extremes from GCM Data. *Water (Basel)* **2019**, *11*, 313. [[CrossRef](#)]
42. Mohr, S.; Kunz, M. Recent trends and variabilities of convective parameters relevant for hail events in Germany and Europe. *Atmos. Res.* **2013**, *123*, 211–228. [[CrossRef](#)]
43. Myoung, B.; Nielsen-Gammon, J. Sensitivity of Monthly Convective Precipitation to Environmental Conditions. *J. Clim.* **2010**, *23*, 166–188. [[CrossRef](#)]
44. Gao, X.; Li, J.; Sorooshian, S. Modeling Intraseasonal Features of 2004 North American Monsoon Precipitation. *J. Clim.* **2007**, *20*, 1882–1896. [[CrossRef](#)]
45. Wang, Y.; Tang, L.; Zhang, J.; Gao, T.; Wang, Q.; Song, Y.; Hua, D. Investigation of Precipitable Water Vapor Obtained by Raman Lidar and Comprehensive Analyses with Meteorological Parameters in Xi'an. *Remote Sens. (Basel)* **2018**, *10*, 967. [[CrossRef](#)]
46. Sim, I.; Lee, O.; Kim, S. Sensitivity Analysis of Extreme Daily Rainfall Depth in Summer Season on Surface Air Temperature and Dew-Point Temperature. *Water (Basel)* **2019**, *11*, 771. [[CrossRef](#)]
47. Liu, Z.; Chen, B.; Chan, S.; Cao, Y.; Gao, Y.; Zhang, K.; Nichol, J. Analysis and modelling of water vapour and temperature changes in Hong Kong using a 40-year radiosonde record: 1973–2012. *Int. J. Climatol.* **2014**, *35*, 462–474. [[CrossRef](#)]
48. Shaw, S.; Royem, A.; Riha, S. The Relationship between Extreme Hourly Precipitation and Surface Temperature in Different Hydroclimatic Regions of the United States. *J. Hydrometeorol.* **2011**, *12*, 319–325. [[CrossRef](#)]
49. Aguilar, E.; Pastor, D.; Vázquez, A.Y.; Ibarra, D. Recolección de datos meteorológicos en tiempo real mediante el uso de funciones asíncronas non-blocking. *Rev. NTHE* **2018**, *24*, 113–117.
50. Gil, S.; Ramírez, G.; Muñoz, M.Y.; González, S. Implementación de un modelo de datos para el almacenamiento de información climatológica en el estado de Querétaro. *Rev. NTHE* **2018**, *24*, 16–19.
51. Vincent, L.; van Wijngaarden, W.; Hopkinson, R. Surface Temperature and Humidity Trends in Canada for 1953–2005. *J. Clim.* **2007**, *20*, 5100–5113. [[CrossRef](#)]
52. Rogers, J.; Wang, S.; Coleman, J. Evaluation of a Long-Term (1882–2005) Equivalent Temperature Time Series. *J. Clim.* **2007**, *20*, 4476–4485. [[CrossRef](#)]
53. Egerer, M.; Lin, B.; Kendal, D. Temperature Variability Differs in Urban Agroecosystems across Two Metropolitan Regions. *Climate* **2019**, *7*, 50. [[CrossRef](#)]
54. Emmanuel, L.; Houngouè, N.; Biaou, C.; Badou, D. Statistical Analysis of Recent and Future Rainfall and Temperature Variability in the Mono River Watershed (Benin, Togo). *Climate* **2019**, *7*, 8. [[CrossRef](#)]
55. Verkade, J.; Brown, J.; Reggiani, P.; Weerts, A. Post-processing ECMWF precipitation and temperature ensemble reforecasts for operational hydrologic forecasting at various spatial scales. *J. Hydrol. (Amst.)* **2013**, *501*, 73–91. [[CrossRef](#)]
56. Yucel, I.; Onen, A.; Yilmaz, K.; Gochis, D. Calibration and evaluation of a flood forecasting system: Utility of numerical weather prediction model, data assimilation and satellite-based rainfall. *J. Hydrol. (Amst.)* **2015**, *523*, 49–66. [[CrossRef](#)]
57. Segond, M.; Onof, C.; Wheeler, H. Spatial-temporal disaggregation of daily rainfall from a generalized linear model. *J. Hydrol. (Amst.)* **2006**, *331*, 674–689. [[CrossRef](#)]
58. Siddique, R.; Mejia, A.; Brown, J.; Reed, S.; Ahnert, P. Verification of precipitation forecasts from two numerical weather prediction models in the Middle Atlantic Region of the USA: A precursory analysis to hydrologic forecasting. *J. Hydrol. (Amst.)* **2015**, *529*, 1390–1406. [[CrossRef](#)]
59. Wu, M.; Lin, G. The very short-term rainfall forecasting for a mountainous watershed by means of an ensemble numerical weather prediction system in Taiwan. *J. Hydrol. (Amst.)* **2017**, *546*, 60–70. [[CrossRef](#)]
60. Bentley, M.; Stallins, J. Synoptic evolution of Midwestern US extreme dew point events. *Int. J. Climatol.* **2008**, *28*, 1213–1225. [[CrossRef](#)]
61. Danladi, A.; Stephen, M.; Aliyu, B.; Gaya, G.; Silikwa, N.; Machael, Y. Assessing the influence of weather parameters on rainfall to forecast river discharge based on short-term. *Alex. Eng. J.* **2018**, *57*, 1157–1162. [[CrossRef](#)]
62. Hofmann, J.; Schüttrumpf, H. Risk-Based Early Warning System for Pluvial Flash Floods: Approaches and Foundations. *Geosciences (Basel)* **2019**, *9*, 127. [[CrossRef](#)]
63. Borsch, S.; Khristoforov, A.; Krovotyntsev, V.; Leontieva, E.; Simonov, Y.; Zatyagalova, V. A Basin Approach to a Hydrological Service Delivery System in the Amur River Basin. *Geosciences (Basel)* **2018**, *8*, 93. [[CrossRef](#)]

64. Chang, C.; Chung, M.; Yang, S.; Hsu, C.; Wu, S. A Case Study for the Application of an Operational Two-Dimensional Real-Time Flooding Forecasting System and Smart Water Level Gauges on Roads in Tainan City, Taiwan. *Water (Basel)* **2018**, *10*, 574. [[CrossRef](#)]
65. Leon, E.; Alberoni, C.; Wister, M.; Hernández-Nolasco, J. Flood Early Warning System by Twitter Using LoRa. *Proceedings* **2018**, *2*, 1213. [[CrossRef](#)]
66. Hoedjes, J.; Kooiman, A.; Maathuis, B.; Said, M.; Becht, R.; Limo, A.; Mumo, M.; Nduhiu-Mathenge, J.; Shaka, A.; Su, B. A Conceptual Flash Flood Early Warning System for Africa, Based on Terrestrial Microwave Links and Flash Flood Guidance. *ISPRS Int. J. Geo Inf.* **2014**, *3*, 584–598. [[CrossRef](#)]
67. Cloke, H.; Pappenberger, F. Ensemble flood forecasting: A review. *J. Hydrol. (Amst.)* **2009**, *375*, 613–626. [[CrossRef](#)]



© 2019 by the authors. Licensee MDPI, Basel, Switzerland. This article is an open access article distributed under the terms and conditions of the Creative Commons Attribution (CC BY) license (<http://creativecommons.org/licenses/by/4.0/>).